RSC Advances

High performance of the Ge@C nanocables as the anode for lithium ion batteries

G. H. Yue[*], X. Q. Zhang, Y. C. Zhao, Q. S. Xie, X. X. Zhang, D. L. Peng[*]

Department of Materials Science and Engineering, Fujian Key Laboratory of Advanced Materials, Xiamen University, Xiamen 361005, China

Abstract: Germanium is a promising high-capacity anode material for lithium ion batteries. But as the huge volume variation always appeared during the charge/discharge process, it usually exhibits poor cycling stability. Herein, a low-cost Ge precursor was used for the preparation of Ge@C core–shell composited NWs by a facile and "green" synthetic route. The Ge@C nanocomposites, as anode materials for lithium-ion batteries, exhibited a high initial discharge capacity of 1648 mAhg^{-1} and superior rate capability. In particular, Ge@C nanocomposite electrodes maintained a reversible capacity of 1086 mAhg^{-1} after repeated cycling at a current density of 0.5 C (600mAg^{-1}) over 200 cycles.

[*]Corresponding author: yuegh@126.com (G. H. Yue); dlpeng@xmu.edu.cn (D.L. Peng). Tel: 86-592-2180155; Fax: 86-592-2183515

1. Introduction

The rapid development of portable electronic devices has drastically increased the demand for lightweight and compact lithium-ion batteries with a high capacity, high rate capability, long cycle lifetime, and high energy-density electrode materials. In order to meet these requirements, development of new electrode materials with higher capacities or higher energy-densities is a pressing need. It has been known for an ideal anode material should provide several demands, such as a high specific capacity, a low potential elative to the counter electrode, long cycling retention, high security, and inexpensive.[1-3] And in these days, alternatives to conventional graphite, numerous lithium alloying materials (i.e., Si, Ge) have been used as anodes, that are capable of exhibiting a high reversible capacity.[4-6]

Germanium, as a promising anode material for lithium ion batteries, has showed some intriguing properties, such as the charming lithium-ion diffusivity (400 times faster than in Si), favorable electrical conductivity (104 times higher than Si), and higher theoretical specific capacity (ca. 1600 mAhg^{-1}, corresponding to $Li_{4.4}Ge$). [7] However, large stresses which were induced by the large volume change, can cause breaking and pulverization of the Ge, leading to bad electrical contact between the active materials and the current collector, and finally led to capacity fading and poor cycling life. To improve this problem, many studies have been conducted to design appropriate anodes by varying the dimensions or morphology,[8, 9] coating the active materials with carbon,[6] and dispersing the active materials into a graphitic matrix.[10–12] J. Cho [13] report Gr/Ge NW(a single to a few layers of graphen on a Ge nanowire) as a Li ion battery anode indicated a long cycle life (200 cycle) and a high specific capacity (1059 mAhg^{-1}) at 4.0

1   C. And these days, there are many reports about the Ge composited nanomaterials were

2   used as the anode for the lithium batteries.[14-22] Especially, Kevin M. Ryan reported the

3   germanium nanowire as anodes shows a excellent rate performance characteristics, a

4   higher capacities (~900 mAh/g), a long cycle life (1100 cycles).[23]

5   And here, the Ge nanowires (NWs) were synthesized with simple PVD methods

6   without any catalyst. Then the Ge@C composited materials were prepared with a simple

7   CVD method. The electrochemical performances of the Ge NWs and Ge@C

8   nanocomposites were evaluated as an anode material for lithium ion batteries (LIBs). And

9   the preparation of Ge@C core–shell nanocomposites shows high rate capability and

10   excellent cycling performance. This technique is environmentally benign and low cost

11   compared to MBE (Molecular beam epitaxy) [24] and MOCVD for synthesis of Ge

12   nanowires. Hence, it is suitable for large-scale synthesis.

13

14   2. Experiments

15   In this study, the Ge NWs were synthesized with a simple PVD method with catalyst

16   free on the copper foils. A conventional two-zone horizontal tube furnace was used for

17   the synthesis. A quartz tube with an outer diameter of 40 mm, inner diameter of 30 mm

18   and length of 800 mm was installed in the furnace. High pure Ge powders (Sigma Aldrich

19   99.99%) (5 g) and the copper foils as the substrate were loaded in the quartz tube in

20   sequence, where the distance between the Ge powder and substrate was about 20 cm. The

21   substrates used were cleaned in dilute HF solution for 30 s and then rinsed in deionized

22   water. And at last, the substrates were dried by a nitrogen gun and placed onto the CVD

23   system. After the quartz tube was evacuated by a vacuum system to about 10^{-3} Pa, the

1   tube was backfilled with a high purity carrier gas of Ar. A procedure was used to control

2   the two-zone heating rate and the start of heating time, respectively. This can make the

3   two zones get their working temperature at 950 and 800℃ at the same time. After that,

4   the temperature of the two zones of the furnace was kept for 60 min, during which the Ar

5   gas with a flow rate of 200 sccm was introduced into the system. After 60 min reaction,

6   the furnace was left to cool down to room temperature with the argon gas. After

7   deposition, the substrate was covered with a black color product.

8   In order to obtain the Ge@C nanocomposite NWs, the as prepared Ge nanowires

9   were moved to another tube furnace. After it had been pulled vacuum for 30 min, the Ar

10   were be refilled into the furnace. After increasing the furnace temperature to 700□, the

11   Argon and acetylene mixed gas flow rate was kept 100 sccm were introduced into the

12   system (In the mixed, the C_2H_2 gas flow volume ratio is 5%) for 10 min. And then

13   cooling to room temperature with the Ar protected.

14   These samples were characterized by X-ray diffraction (XRD, D/Max-2400x, CuK_a

15   radiation), and field-emission scanning electron microscopy (FE-SEM, FEI Nano230).

16   Energy dispersive X-ray spectroscopy (EDS) attaching to FE-SEM was used to analyze

17   the elemental composition of the samples. Before high resolution transmission electron

18   microscopy (HRTEM, JEOL JEM-2100F) observation, the samples (NWs) were scraped

19   off   from the substrates and then suspended into ethanol solution.

20   The electrochemical properties were carried out by two-electrode cells with lithium

21   metal as the counter and reference electrodes at room temperature. A slurry was prepared

22   by mixing the active material (Ge NWs or Ge@C nanocomposite), carbon black,

23   polyacrylic acid (PAA), and carboxymethyl cellulose (CMC) in a weight ratio of

1   80:10:5:5. And then paste the slurry on a Cu foil using the doctor-blade method. Finally, a

2   lithium foil (reference electrode), a polyethylene separator, and an electrolyte solution of

3   1.3m $LiPF_6$ in ethylene carbonate/ethyl methyl carbonate (wt% 3:7) with 10% of Fluor

4   ethylene carbonate (Panax Starlyte) were be assembled to the half cell. The slurry which

5   were loading amount on the Cu foil was ranged from 1.0 to 1.9 mg cm^{-2}. The specific

6   capacity was detected within a voltage window between 0.001 and 1.5 V at various

7   C-rates. The mass of the active anode material were be using to calculate the specific

8   capacity. Cyclic voltammetry was conducted at a scan rate of 0.1 mV s^{-1}.

9

3. Results and Discussion

11   Fig.1a shows the powder X-ray diffraction (XRD) patterns of the Ge NWs and the

12   Ge@C NWs nanocomposite. Five main peaks at 27.41°, 45.47°, 53.58°, 66.51°, and

13   72.64° can be detected in the XRD patterns of both the Ge NWs and the Ge@C NWs

14   nanocomposite, which corresponded to the (111), (220), (311), (400), and (331)

15   reflections of cubic Ge, respectively (JCPDS Card No. 65-0333, space group *Fd3m*

16   (227)). For both samples, it also can be found that the sharp and symmetrical diffraction

17   peaks indicated that the Ge NWs with a good crystalline phase, and it is also confirmed

18   that the carbon is amorphous for there was no diffraction peak of carbon in the Ge@C

19   nanocomposite.

20   And further structural information is provided by the Raman spectra. Fig. 1b

21   exhibits the Raman spectrum of the Ge NWs and the Ge@C NWs nanocomposite. And to

22   our knowledge that the two peaks were observed at ~1350 and 1590 cm^{-1} are

23   corresponding to the D band and G band, respectively.[25] The crystalline of the carbon

1   materials will decided the relative peak area ratios and sharpness of the D and G band

2   peaks, and from this figure the stronger D band and broad peaks indicate that amorphous

3   carbon is coated on the Ge NWs. Additionally, a peak at ~300 cm^{-1} was noticeable, which

4   is indicative of Ge–Ge vibration. Also, even after carbon coating, GeO$_x$ formation was

5   not observed. Moreover, the Raman spectrum of the Ge@C NWs shows a little Red shift

6   maybe caused by the carbon shell.

7

8   Fig. 2 shows the typical FESEM and TEM images of the bare Ge NWs and the

9   Ge@C nanocomposite. The overall morphology of the bare Ge NWs is shown in Fig.

10   2(a). From this image, it can be seen that the as-synthesized Ge nanowires are almost

11   totally composed of uniform nanowires and in which nanowires of different sizes that

12   bend and entwine each other could be found. Some Ge nanoparticles can be detected in

13   this image, and these particles can explain the growth mechines of the Ge NWs (See

14   Supporting information). Fig. 2(b) shows a SEM image of the carbon sheathed Ge NWs,

15   and the morphology of the Ge@C NWs was sustained after carbon coating. The Fig. 2(c)

16   was the TEM image of the Ge@C nanocomposite, it was can be find that the nanowires

17   are uniform with a diameter about 30~50 nm and the length about several micrometer.

18   And the insert in the Fig. 2(c) is the high magnification image images of the Ge@C

19   nanocomposite, and it confirmed that the Ge NWs was covered with the amorphous

20   carbon shell. Further insight into the structure of the Ge@C nanocomposite is obtained

21   from high-resolution transmission electron microscopy (HRTEM) recorded on an

22   individual nanowire. The HRTEM of Ge@C nanocomposite exhibits that the Ge NWs

23   with a good crystalline and continuous lattice fringes over a large area, this image clearly

1   reveals that the as-synthesized Ge nanowire has no defect of dislocation. The interplanar

2   spacing is 0.32 nm, which corresponds to the *d* (111) spacing for the cubic (space group

3   *Fd3m* (227)) structure, confirming the crystalline nature of the produced Ge nanowires.

4   The thickness of the amorphous carbon shell also can be provided from the HRTEM is

5   about 7 nm. And an EDS line profile of Ge (Green) and C (Blue) along the red line can

6   be found in Figure S3. The amount of carbon in the Ge@C NWs was 10 wt%, as

7   measured by a Thermogravimetric analyzer. Thermogravimetric analysis (TGA) results

8   showed the Ge@C composite to contain ~80 wt % Ge (See Figure S4).

9

10   Fig. 3 exhibits the voltage profiles of the Ge NWs, and the discharge and charge

11   capacity of the first cycle were 2093 mAh g^{-1} and 1506 mA h g^{-1} in the range of 0 V and

12   1.5 V vs. Li/Li$^+$ at the rate of 0.5 C (600 mA g^{-1}), which is much higher than the

13   theoretical value of 1600 mAh g^{-1} for Ge. Similar observation was also reported [26, 27],

14   and it was attributed to the initial reactions at the surface of the Ge NWs, formation of

15   surface electrolyte interphase (SEI), [28] leading to higher discharge capacity being

16   observed. But the bare Ge NWs exhibit significantly decreased of the specific capacity.

17   Its charge capacity at the 30th cycles is 468 mAh g^{-1}, and the discharge capacity is 496

18   mAh g^{-1}. The significantly decreased irreversible capacity of the Ge NWs is believed to

19   be resulted from the decreased formation of the non-conducting solid–electrolyte

20   interface (SEI).[28] And for this phenomenon has been reported that the irreversible

21   capacity of the lithium reactive alloys is closely related to the intensive side reactions

22   between the active material and electrolyte species (especially LiPF6).[29, 30]

23

1   Fig. 4(a) shows the voltage profiles of the Ge@C NWs versus lithium at a cycling

2   rate of 0.5 C (600 mAg^{-1}) between 0 and 1.5 V. And the CV profiles of the Ge@C

3   composited NWs electrode at a scan rate of 0.1 mVs^{-1} within the voltage range 0.01 – 1.5

4   V versus Li/Li^{+} were indicated with an excellent electrochemical reversibility (See Figure

5   S5). For the first cycle, the discharge and charge capacity were 1648 mAhg^{-1} and 1332

6   mAhg^{-1}, respectively, corresponding to a coulombic efficiency of 80%. Thus, for the

7   Ge@C NWs sample, the discharge capacity, if based only on Ge, is 1831 mAh g^{-1}, which

8   is close to the value of bare Ge NWs.[27] It is well known that the SEI formed during the

9   first charging step and which led to the detected specific capacity is higher than the

10   theoretical capacity value (1600 mAhg^{-1}) with a coulombic efficiency of 80% at the first

11   charging. And in the second cycle, the discharge and charge capacity decreased rapidly to

12   1341 mAhg^{-1} and 1229 mAhg^{-1}. This phenomenon can be explained as above of the bare

13   Ge NWs. And then, the Ge@C NWs shows a long cycle life and high specific capacity at

14   0.5 C. From Fig. 4(a), it can be found that the discharge and charge capacity changed to

15   steady decline and reduced very slowly. From this figure, it can be found that at the 200th

16   cycle the discharge and charge capacity were 1088 mAh g^{-1} and 1086 mAh g^{-1}. Our

17   Ge@C NWs shows noticeably improved efficiency, which may be due to the carbon

18   coating which minimized surface oxidation of germanium NWs. The coulombic

19   efficiency increased to 91% and 93% very rapidly at the second and third cycle,

20   respectively. And the Fig. 4(b) indicated that the coulombic efficiency begins to display a

21   stable value ranging around 99% from the 4th cycle to the 200th cycle, which indicates that

22   the Ge@C NWs has an remarkable reversibility in charging and discharging by Li^{+} ions

23   after the SEI is formed.

In the process of the charging and discharging process, the Ge structure will be destruction as the volume expansion. And this is the main reason that most of the degradation of the Ge anode materials. Here, the long cycle life with higher capacity retention of the Ge@C NWs maybe owed to intimate contact between the Ge nanowires and carbon as the Ge nanowires were holded tightly with the carbon to accommodate the mechanical strain effectively. Furthermore, for the Ge@C NWs sample, the core of Ge nanowires were growth directly by CVD methods without any catalyst in our experimental, And as the growth mechanisms mentioned that the Ge nanoparticles fromed in supporting information, and the Ge nanowires were formed with the Ge separate out from the Ge nanoparticles after absorbing the Ge gas and reach supersaturated. So, the Ge nanoparticles maybe acted as the excellent electron communication between the Ge@C composited NWs and electrolyte solution during the cycles. Once again, here the Ge nanoparticles maybe as the buffered section to provide facile strain relaxation to accommodate the volume variations during lithiation/delithiation in the hybrid nanostructural composed of nanoparticles and nanowires with greatly improved cycle life and rate capability. [31]

In Fig. 5, the rate capabilities detected for both the bare Ge NW and the Ge@C NWs from 0.1 to 10 C. As mentioned above, the Ge@C NWs sample shows an charming rate capability even at a higher C-rate. For instance, the specific capacity of the Ge@C NWs is about 583 mAhg^{-1} at 10 C (=12 A g^{-1}). Moreover, the specific capacity of the Ge@C NWs is about 181 mAhg^{-1} at 20 C (=24 A g^{-1}). But, in the case of a bare Ge NW, the specific capacity reduces quickly upon the C-rate increased from 0.1 to 10 C and with a

1   specific capacity of 18 mAh g^{-1} at 10 C. It is noted that the voltage profiles for the rate

2   capability of the Ge@C NWs are shown in Figure 5(b). The improved rate performance

3   is attributed to the morphology of the nanowires. It is well known that during the heating

4   process for carbon coating, the nanoparticles become agglomerated and grow, and which

5   lead to inhomogenous carbon coating. But, nanowires as the one dimensional

6   nanomaterials are not easy to aggregate in parallel. Therefore, the agglomeration of

7   nanowires is inhibited effectively during carbon coating, resulting in homogeneous

8   carbon coating.

9

10   Fig. 6(a) shows that the SEM (See figure S6) and TEM image of the Ge@C

11 composited NWs after 200 cycles. It is indicated that the pristine crystalline phase was

12 transformed gradually into an amorphous phase, which also was reported by Chan [26].

13 Also, after 200 cycles, the diameter of the Ge NWs increased to about 150 nm for lithium

14 de/insertion, which was about 5 times greater than the pristine sample (Fig. 2(c)), as

15 expected from the predicted volume change, and this means that Ge@C NWs have a

16 quite porous structure. Remarkablely, The Ge grains may be either pristine Ge that was

17 never lithiated (and can be led to the darker contrast region observed in the core of the

18 nanowire in Fig. 6(a)) or Ge that recrystallized under delithiation, which has been

19 observed in thin films. [32]. And the Ge element distribution of the Ge@C NWs after 200

20 cycles and line mapping of Ge along the yellow line was shown in Fig. 6(b). It is also

21 noteworthy that are different with the reactions of Ge thin films and nanoparticles, the

22 Ge@C NWs were not cracked after cycling and that they preserved their own nanowire

23 morphology.[33, 34] The robustness of the Ge@C NWs seems to be caused by avoiding a

1   two phase reaction. Crystalline Ge NWs transformed into amorphous Ge NWs during

2   cycling. Therefore, during electrochemical de/alloying process, a homogenous volume

3   change of electrode materials made the local stress gradients suppressed, and which

4   resulting in the inhibition of cracking and pulverization also.[6] And it is also can be

5   found that there are some Ge nanoparticles can be detected on the NWs, with the point

6   analyzing. It is confirmed our speculation that the Ge nanoparticles were acted as the

7   electron communication and buffered section during the cycles. And compared to

8   previous similar works, we listed a table about the capacitive of different Ge

9   nanocomposites. we can see that the Ge NWs in this work exhibits the highest capacity

10   after 100 cycle. Moreover, the coulombic efficiency is relatively high, because mass of

11   SEI layer format due to the possible less irreversible processes, when first discharge takes

12   place.

13

14   **Conclusions**

15   The Ge NWs were prepared with a simple PVD process without any catalyst

16   involved. And then the carbon grows directly on the surface of Ge NWs to forming the

17   Ge@C nanocomposited. SEM and TEM analyses confirmed the core–shell

18   nanoarchitecture of the Ge@C composited NWs, with the length about several

19   micrometers to a dozen even dozens of micrometer. Individual Ge NWs were coated by a

20   continuous carbon layer, which had an average thickness of 7 nm. The composite

21   electrode composed of single crystalline Ge NWs sheathed with amorphous carbon

22   showed excellent electrochemical properties of large reversible capacity, high coulombic

23   efficiency (1086 mAhg^{-1}) at 0.5 C-rate, excellent rate capability and stable cycle

24   performance (200 cycle) at a higher capacity retention (90%).   The improved

1 electrochemical performance of Ge@C NWs fabricated in this experiment is attributed to

2 the formation of amorphous Ge NWs during cycling, inhibition of surface oxidation of

3 the Ge NWs and a homogenous carbon coating on discrete Ge NWs. These results

4 suggest that the use of nanowire structure can be promising for alloy anode materials in

5 lithium ion batteries.

6

7 **Acknowledgements**

12

Reference

1. P. G. Bruce, B. Scrosati, J. M. Tarascon, *Angew. Chem. Int. Ed.*, **47** (2008) 2930.

2. C. Liu, F. Li, L.-P. Ma, H. M. Cheng, *Adv. Mater.*, **22** (2010) E28.

3. H. Wu, Y. Cui, *Nano Today*,   **7** (2012) 414.

4. C. K. Chan, H. Peng, G. Liu, K. McIlwrath, X. F. Zhang, R. A. Huggins, Y. Cui, *Nat. Nanotechnol.*, **3** (200) 31.

5. M. S. Park, G. X. Wang, Y. M. Kang, D. Wexler, S. X. Dou, H. K. Liu, *Angew. Chem. Int. Ed.*, **46** (2007) 750.

6. M. H. Seo, M. Park, K. T. Lee, K. Kim, J. Kim, J. Cho, *Energy Environ. Sci.*, **4** (2011) 425.

7. M. Park, Y. Cho, K. Kim, J. Kim, M. Liu, and J. Cho, *Angew. Chem. Int. Ed.*, **50** (2011) 9647.

8. H. Zhang and P. V. Braun, *Nano Lett.*, **12** (2012) 2778.

9. H. Kim, B. Han, J. Choo, and J. Cho, *Angew. Chem. Int. Ed.*, **47** (2008) 10151.

10. D. J. Xue, S. Xin, Y. Yan, K. C. Jiang, Y. X. Yin, Y. G. Guo, and L. J. Wan, *J. Am. Chem. Soc.*, **134** (2012) 2512.

11. B. Li, H. Cao, J. Shao, and M. Qu, *Chem. Commun.*, **47** (2011) 10374.

12. Z. S. Wu, W. Ren, L.Wen, L. Gao, J. Zhao, Z. Chen, G. Zhou, F. Li, and H. M. Cheng, *ACS Nano*, **4** (2010) 3187.

13. H. Kim, Y. Son, C. Park, J. Cho, and H. C. Choi, *Angew. Chem.*, **125** (2013) 6113.

14. J. Ren, Q. Wu, H. Tang, G. Hong, W. Zhang and S. Lee, *J. Mater. Chem. A*, **1** (2013) 1821.

15. A. M. Chockla, K. C. Klavetter, C. B. Mullins, and B. A. Korgel, *ACS Appl. Mater. Interfaces*, **4** (2012) 4658.

16. Y. J. Cho, H. S. Im, H. S. Kim, Y. Myung, S. H. Back, Y. R. Lim, C. S. Jung, D. M. Jang, J. Park, E. H. Cha, W. Cho, F. Shojaei, and H. S. Kang, *ACS Nano*, **7** (2013) 9075.

17. F. Yuan, H. Yang, and H. Tuan, *ACS Nano*, **6** (2012) 9932.

18. C. K. Chan, X. F. Zhang, and Y. Cui, *Nano Lett.*, **8** (2008) 307.

19. J. G. Ren, Q. Wu, H. Tang, G. Hong, W. Zhang, and S.T. Lee, *J. Mater. Chem. A*, **1** (2013) 1821.

20. S. Hwak Woo, S. J. Choi, J. Park, W. Yoon, S. W. Hwang, and D. Whang, *J. Electrochem. Soc.*,

160 (2013) A112.

21. D. Li, K. H. Seng, D. Shi, Z. Chen, H. K. Liu and Z. Guo, *J. Mater. Chem. A*, **1 (**2013) 14115.

22. C. Wang, J. Ju, Y. Yang, Y. Tang, J. Lin, Z. Shi, R. P. S. Han and F. Huang, *J. Mater. Chem. A*, **1** (2013) 8897.

23. N.D. Zakharov, P. Werner, G. Gerth, L. Schubert, L. Sokolov, U. Gösele, *J. Crystal Growth*, **290** (2006) 6

24. T. Kennedy, E. Mullane, H. Geaney, M. Osiak, C. O'Dwyer, and K. M. Ryan, *Nano Lett.*, Just Accepted Manuscript • DOI: 10.1021/nl403979s.

25. Y. Wang and G. Wang, *Chem. Asian J.*, **8** (2013) 3142.

26. C. K. Chan , X. F. Zhang, and Y. Cui, *Nano Lett.*, **8** (2008) 307.

27. L. P. Tan, Z. Y. Lu, H. T. Tan, J. X. Zhu, X. H. Rui, Q. Y. Yan, H. H. Hng, *J. Power Sources,* **206** (2012) 253.

28. J. Cho, *J. Mater. Chem*., **20** (2010) 4009.

29. D. Aurbach, A. Nimberger, B. Markovsky, E. Levi, E. Sominski and A. Gedanken, *Chem. Mater*., **14** (2002) 4155.

30. H. Uono, B. C. Kim, T. Fuse, M.Ue, J. I. Yamaki, *J. Electrochem. Soc*., **153** (2006) A1708.

31. L. Q. Mai , Q. Wei , Q. An , X. Tian , Y. Zhao , X. Xu , L. Xu ,L. Chang , and Q. Zhang, *Adv. Mater*., **25** (2013) 2969.

32. J. Graetz, C. C. Ahn, R. Yazami, B. Fultz, *J. Electrochem. Soc.*, **151** (2004) A698.

33. H. Lee, H. Kim, S. G. Doo and J. Cho, *J. Electrochem. Soc*., **154** (2007) A343.

34. J. Graetz, C. C. Ahn, R. Yazami and B. Fultz, *Electrochem. Solid-State Lett.*, **151** (2004) A698.

35. J. G. Ren, Q. H.Wu, H. Tang, G. Hong, W. J. Zhang and S. T. Lee, *J. Mater. Chem. A*, **1** (2013) 1821.

36. C. Wang, J. Ju, Y. Q. Yang, Y. F. Tang, J. H. Lin, Z. J. Shi, F. Q. Huang, *J. Mater. Chem. A*, **1** (2013) 8897.

37. K. H. Seng, M. Park, Z. P. Guo, H. K. Liu, and J. Cho, *Angew. Chem. Int. Ed.* **51**(2012)5657.

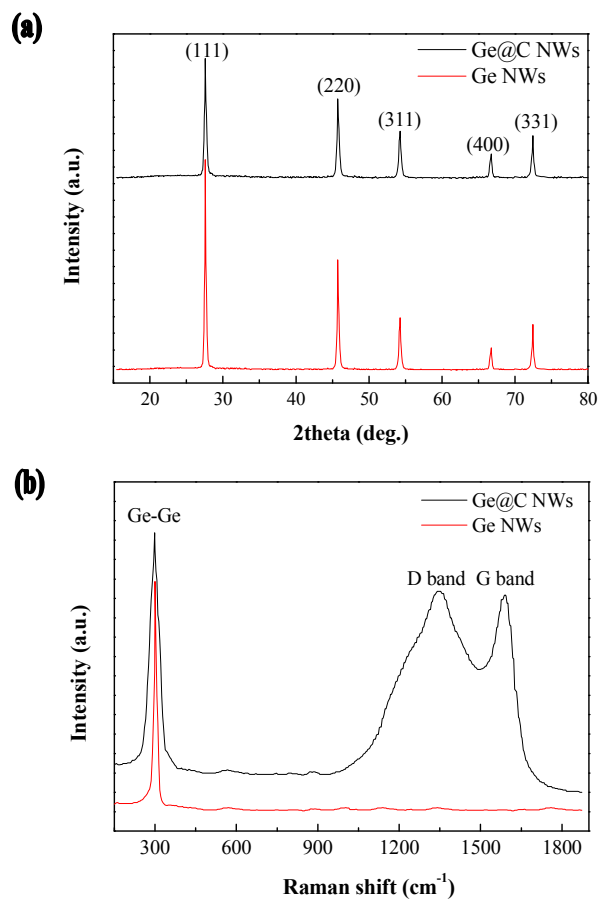# List of Figures Caption and Table

Fig. 1 XRD patterns and Raman spectrum of the Ge NWs and Ge@C NWs nanocomposite.
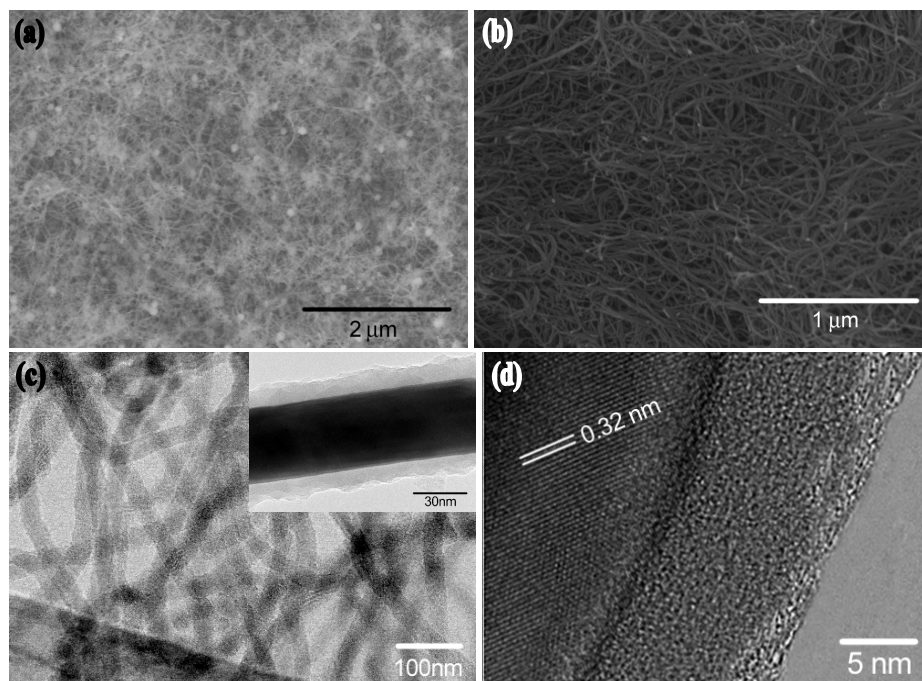
Fig. 2. (a) SEM image of the as prepared Ge NWs, (b) SEM image of the Ge@C NWs nanocomposited, (c) TEM image of the Ge@C NWs, and the insert is the zoom in image, (d) HR-TEM images of the Ge@C NWs.
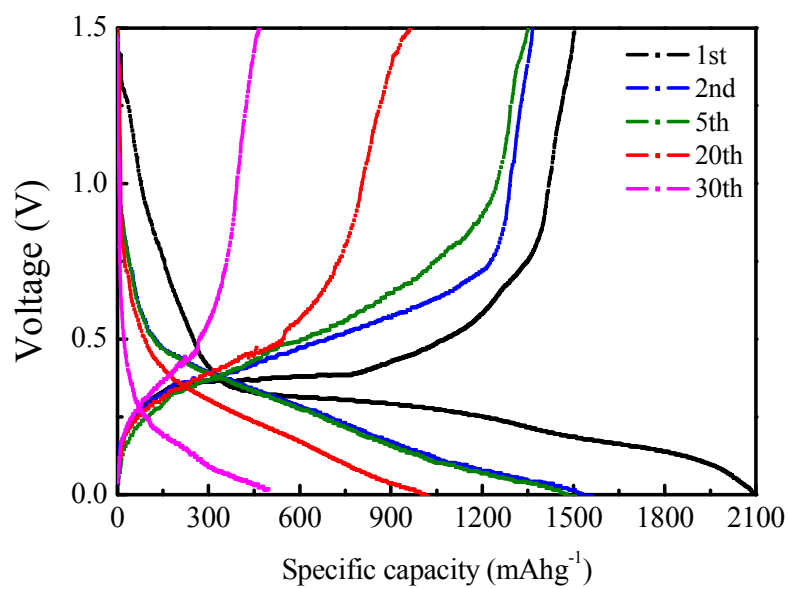
Fig. 3 Galvanostatic charge/discharge profiles of Ge NWs for selected cycles at the current density of 0.5C (600 mA g^{-1}), in the potential window from 0.01 V to 1.5 V.
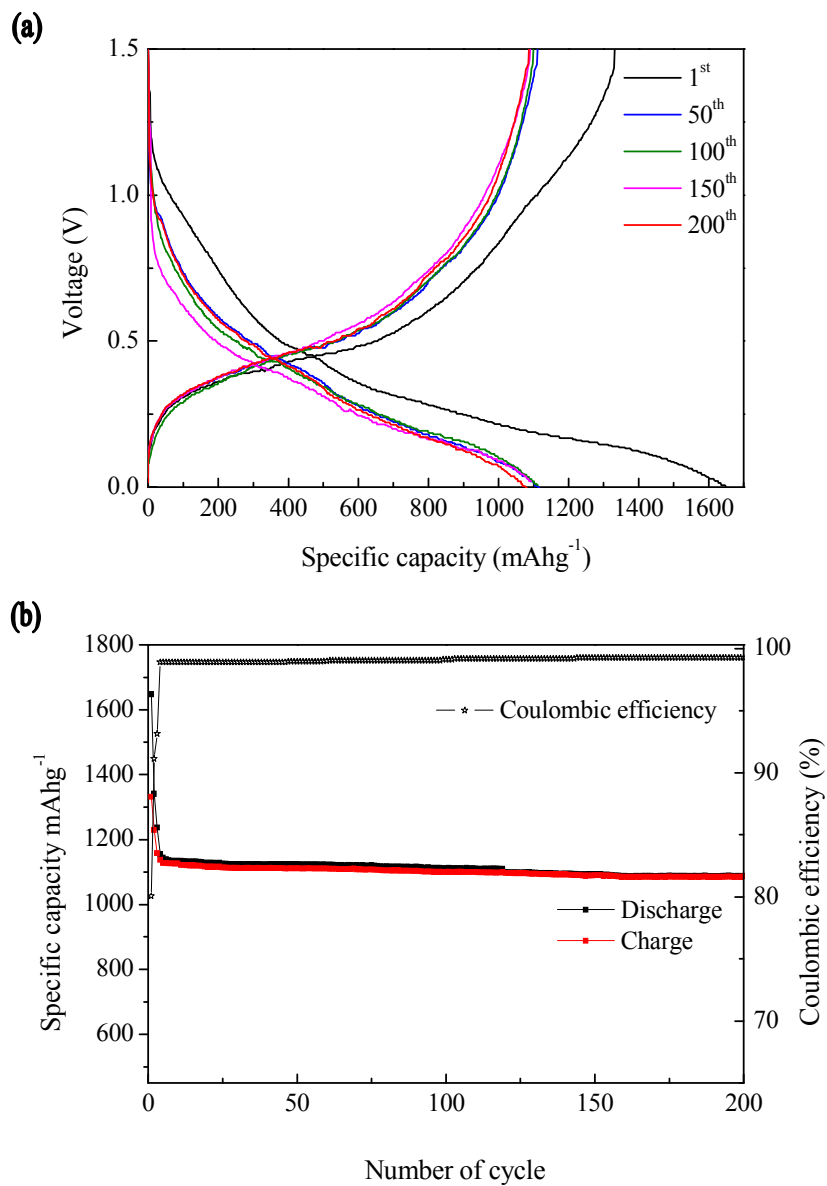
Fig. 4. (a) Voltage profiles of a Ge@C NWs between 0 and 1.5 V at a rate of 0.5C. (b) Cycle performance of a Ge@C NWs and coulombic efficiency at a rate of 0.5 C.
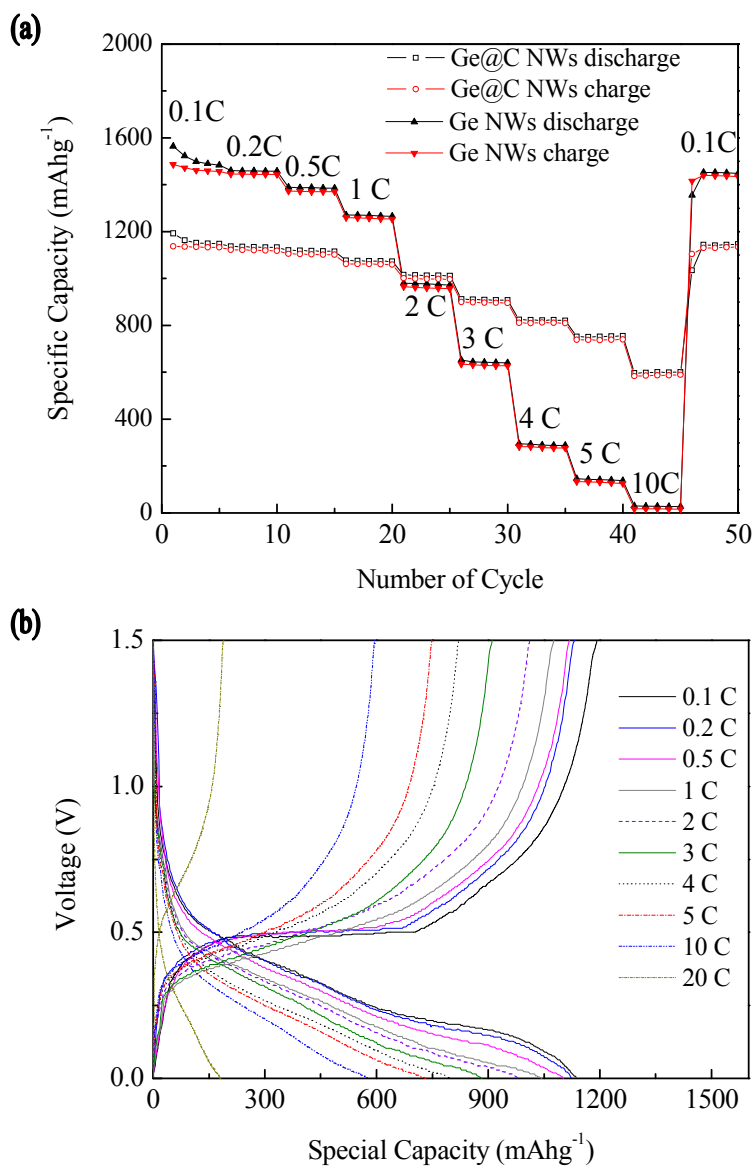
Fig. 5. (a) Rate capability of a Ge@C NWs and a bare Ge NW from 0.1 to 10 C. (b) Voltage profiles of the Ge@C NWs corresponding to the rate capability measurement in (a).
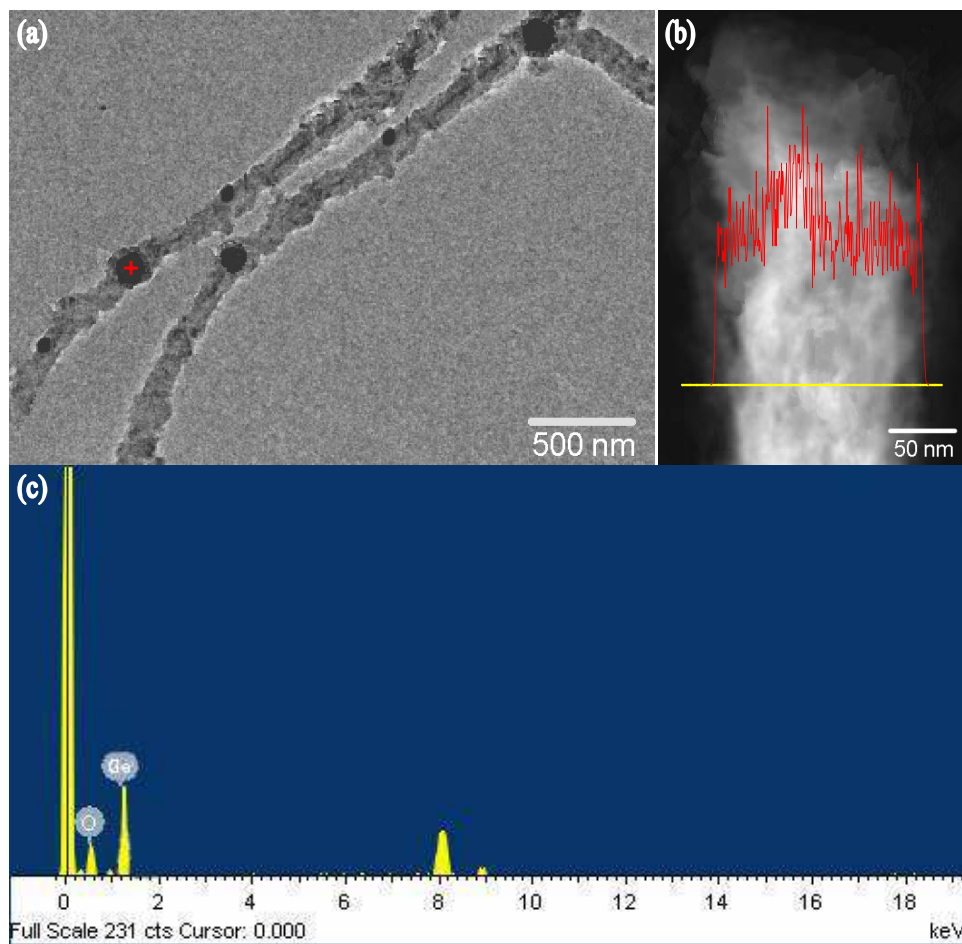
Fig. 6. (a) TEM image of c-Ge-NW after 200 cycles, (b) expanded image of (b) and line mapping of Ge along the yellow line, and (c) is the point elements analyzed of the red mark of (a).

Table 1 Comparison of electrochemical performance of Ge@C NWs as anode material for the LIBs

Fig. 1 XRD patterns and Raman spectrum of the Ge NWs and Ge@C NWs nanocomposite.

Fig. 2. (a) SEM image of the as prepared Ge NWs, (b) SEM image of the Ge@C NWs nanocomposited, (c) TEM image of the Ge@C NWs, and the insert is the zoom in image, (d) HR-TEM images of the Ge@C NWs.

Fig. 3 Galvanostatic charge/discharge profiles of Ge NWs for selected cycles at the current density of 0.5 C (600 mA g^{-1}), in the potential window from 0.01 V to 1.5 V.

Fig. 4. (a) Voltage profiles of a Ge@C NWs between 0 and 1.5 V at a rate of 0.5C. (b) Cycle performance of a Ge@C NWs and coulombic efficiency at a rate of 0.5 C.

Fig. 5. (a) Rate capability of a Ge@C NWs and a bare Ge NW from 0.1 to 20 C. (b) Voltage profiles of the Ge@C NWs corresponding to the rate capability measurement in (a).

Fig. 6. (a) TEM image of c-Ge-NW after 200 cycles, (b) expanded image of (b) and line mapping of Ge along the yellow line, and (c) is the point elements analyzed of the red mark of (a).

Table 1 Comparison of electrochemical performance of Ge@C NWs as anode

material for the LIBs

Materials	Current density (mA g⁻¹)	After 100 cycle discharge specific capacity (mAh g⁻¹)	Initial coulombic efficiency (%)	Ref.
Ge/graphene	200	400	48	35
Ge@G	1600	410	53	36
NC-Ge/C	800	870	70	37
Ge@C NWs	800	1150	80	This work

Supporting information

High performance of the Ge@C nanocables as the anode for lithium ion batteries

G. H. Yue*, X.Q. Zhang, Y. C. Zhao, Q. S. Xie, X. X. Zhang, D. L. Peng*

Department of Materials Science and Engineering, Fujian Key Laboratory of Advanced

Materials, XiamenUniversity, Xiamen 361005, China

To whom correspondence should be addressed. E-mail: yuegh@126.com (G. H. Yue);

dlpeng@xmu.edu.cn (D.L. Peng)

Growth mechanism of the Ge NWs

In our experiment, there without any catalysis, and there are many nanoparticles can be seen from the SEM images. The EDS spectrum indicated that the particles are Ge nanoparticles (Figure S1 & Fig. 2(a)). If we shorter the reaction time, the tadpole-looking products can be detected. And as the reaction time longer, the Ge NWs can be obtained. So, the growth mechanism should be speculated as the following:

First, the Ge gas had been absorbed with the substrate and rapid nucleation and growth. And then the Ge nanoparticles stop growing as it grows up to some dimension scope. Then the Ge nanoparticles with absorbing over-saturated Ge gas and begin to separate out Ge element to forming the Ge NWs.

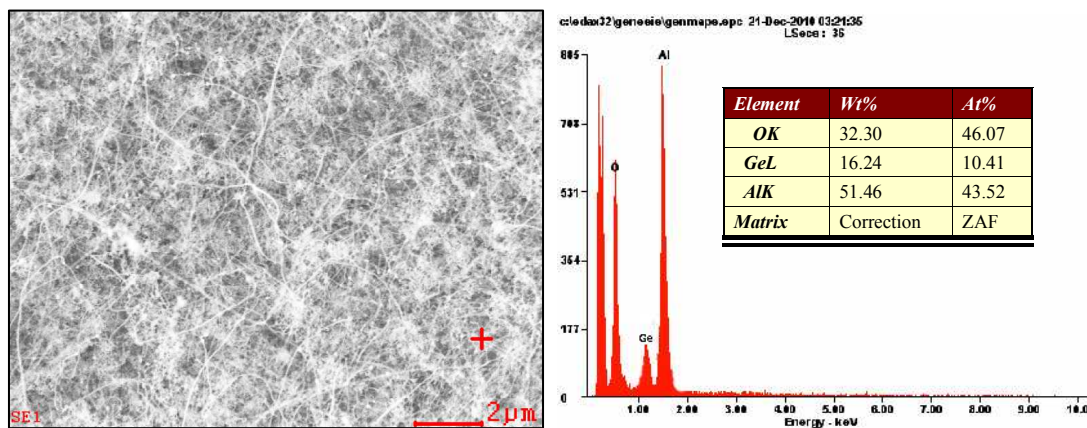| Element	Wt%	At%
OK	32.30	46.07
GeL	16.24	10.41
AlK	51.46	43.52
Matrix	Correction	ZAF

Figure S1. The SEM images of the as prepared Ge NWs on the sapphire substrate, the right side is the EDS image of the red mark in the SEM image and the insert is the element analysis of the EDS image.
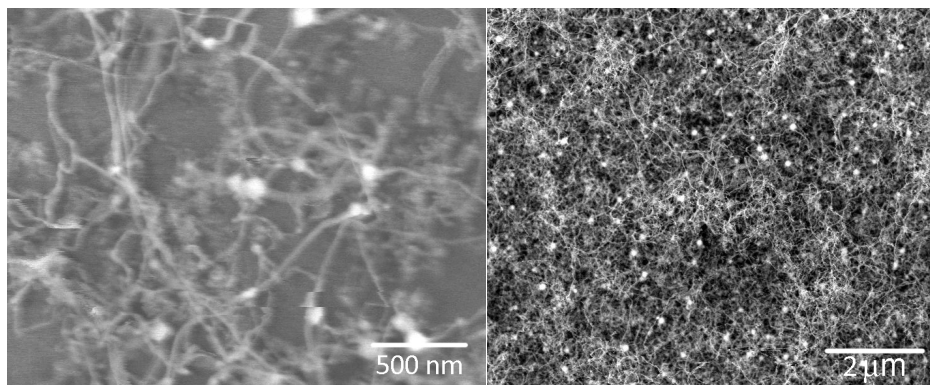
Figure S2. The Ge NWs growth on the sapphire substrate with different growth time, the left is 10 min and the right is 60 min.
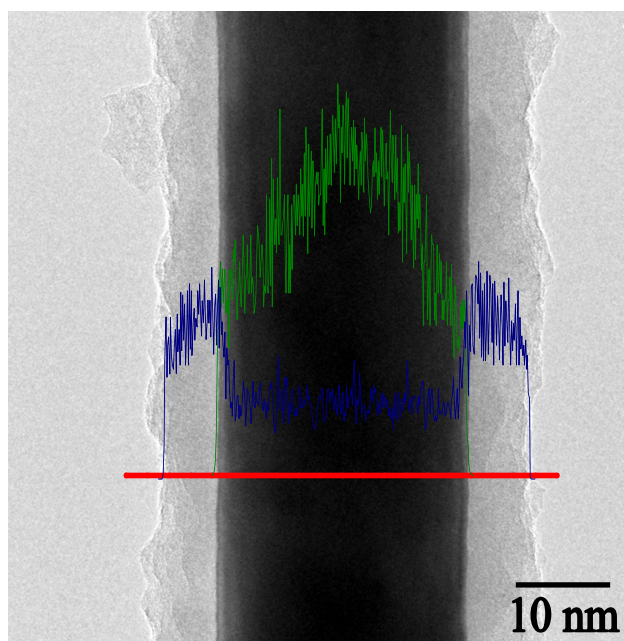

Figure S3. TEM image of Ge@C NW and EDS line profiles of Ge (Green) and C (Blue) along the red line.

Thermogravimetric analysis (TGA), carried out in air at a heating rate of 10 °C min^{-1}, was used to determine the chemical composition of the Ge@C composite NWs.

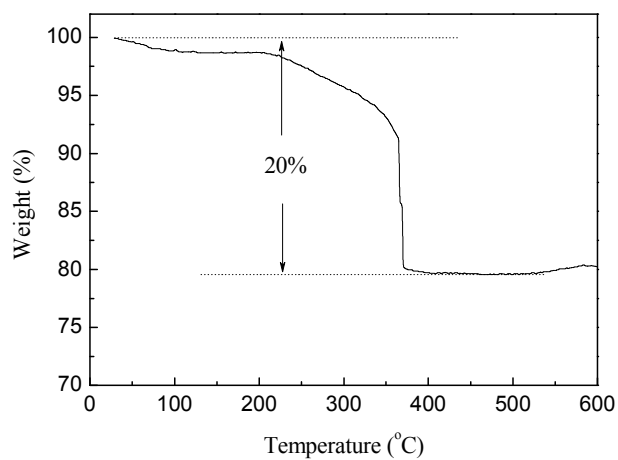The results showed the Ge@C composite to contain ~80 wt % Ge.

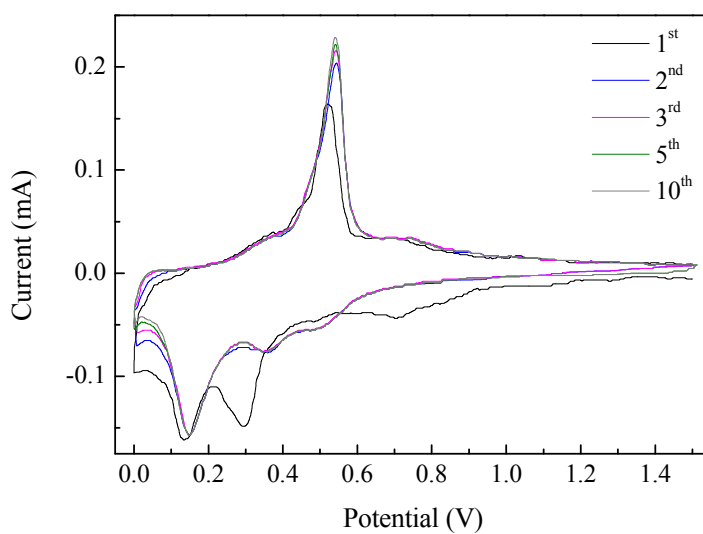Figure S 4. Thermogravimetric analysis (TGA) of Ge@C NWs in air.

Figure S5. CV profiles of the Ge@C composited NWs electrode at a scan rate of 0.1 mVs^{-1} within the voltage range 0.01−1.5 V versus Li/Li^{+}.

Cyclic voltammetry (CV) was performed to understand the redox properties of the

Ge@C composited NWs as an anode material in lithium-ion cells. Two extra reduction peaks at 0.8 and 0.3 V were observed in the first scanning cycle, which could be associated with the formation of a solid electrolyte interphase (SEI) layer. During the subsequent discharge process, the three peaks centered at 0.5, 0.36, and 0.15 V corresponded to multistep reactions between Ge and Li. The reduction of Ge could proceed as $4.4Li^+ + Ge + 4.4e^- \rightarrow Li_{4.4}Ge$, based on complete lithiation. Upon charging, one sharp and symmetrical peak at 0.53 V was observed, which corresponded to the oxidation of Li$_x$Ge into Ge. Moreover, the positions and intensities of the redox peaks remained unchanged during the second cycle, thus suggesting that the Ge@C composited NWs electrode has excellent electrochemical reversibility.
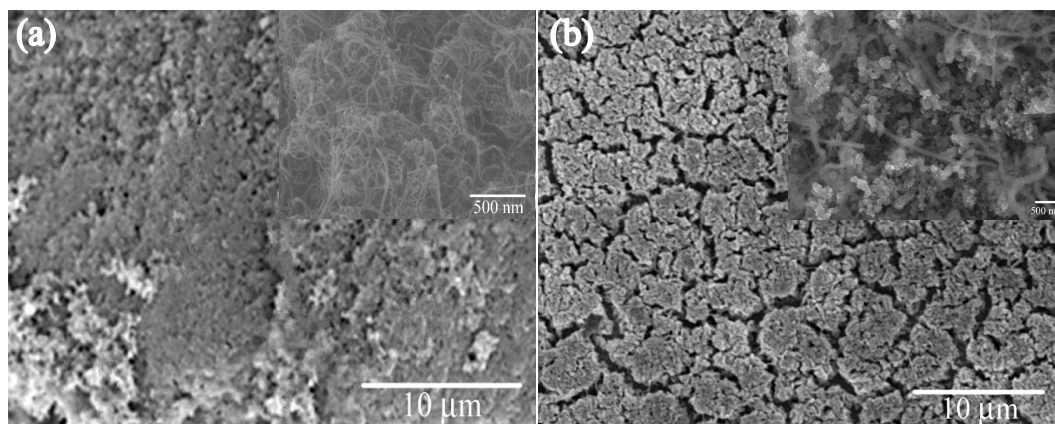

Figure S6. SEM images of the surface of Ge@C composites NWs electrodes before cycles (a) and after (b) 200 cycles at 0.5 C.

In figure S6, it can be found that the Ge@C composite NWs were volume expanded or broken into powder-like after the 200 cycles at 0.5C. And the diameter of the Ge NWs was about 5 times greater than the pristine sample for lithium de/insertion.